

Purveyors of fine halos

III. Chemical abundance analysis of a potential ω Cen associate[★]

Andreas J. Koch-Hansen¹, Camilla Juul Hansen², Linda Lombardo³, Piercarlo Bonifacio³, Michael Hanke¹, Elisabetta Caffau³

¹ Zentrum für Astronomie der Universität Heidelberg, Astronomisches Rechen-Institut, Mönchhofstr. 12, 69120 Heidelberg, Germany

² Max-Planck Institut für Astronomie, Königstuhl 17, 69117 Heidelberg, Germany

³ GEPI, Observatoire de Paris, Université PSL, CNRS, 5 Place Jules Janssen, 92190, Meudon, France

ABSTRACT

Globular clusters (GCs) are important donors to the build-up of the Milky Way (MW) stellar halo, having contributed at the ten percent level over the Galactic history. Stars that originated from the second generation of dissolved or dissolving clusters can be readily identified via distinct light-element signatures such as enhanced N and Na and simultaneously depleted C and O abundances. In this paper we present an extensive chemical abundance analysis of the halo star J110842, which was previously kinematically associated with the massive MW GC ω Centauri (ω Cen), and we discuss viable scenarios from escape to encounter. Based on a high-resolution, high signal-to-noise spectrum of this star using the UVES spectrograph, we were able to measure 33 species of 31 elements across all nucleosynthetic channels. The star's low metallicity of $[\text{Fe}/\text{H}] = -2.10 \pm 0.02(\text{stat.}) \pm 0.07(\text{sys.})$ dex places it in the lower sixth percentile of ω Cen's metallicity distribution. We find that all of the heavier-element abundances, from α - and Fe-peak elements to neutron-capture elements are closely compatible with ω Cen's broad abundance distribution. However, given the major overlap of this object's abundances with the bulk of all of the MW components, this does not allow for a clear-cut distinction of the star's origin. In contrast, our measurements of an enhancement in CN and its position on the Na-strong locus of the Na-O anticorrelation render it conceivable that it originally formed as a second-generation GC star, lending support to a former association of this halo star with the massive GC ω Cen.

Key words. Galaxy: abundances — Galaxy: formation — Galaxy: globular clusters: general — globular clusters: individual: ω Cen — Galaxy: halo — Galaxy: stellar content

1. Introduction

The stellar halo of the Milky Way (MW) galaxy conceivably formed through a variety of channels. Thus, in situ star formation within the host galaxy is contrasted by an ex situ formation, where the halo stars were born in satellite galaxies and accreted onto the host system only later on. The purported relative importance of either scenario varies in the literature and it is currently believed that our Galaxy experienced a mixture of both, where the ex situ component contributed to different degrees depending on galactocentric radius (Eggen et al. 1962; Searle & Zinn 1978; Dekel & Silk 1986; Bullock & Johnston 2005; Zolotov et al. 2009; Cooper et al. 2013; Pillepich et al. 2015; Naidu et al. 2020).

One important class of donors to the buildup of the MW halo is the globular clusters (GCs), and there is a wealth of evidence for their ongoing tidal disruption and for their accretion, ranging from observations of stellar streams (e.g., Odenkirchen et al. 2001; Lee et al. 2004) and extended envelopes of present-day GCs (e.g., Jordi & Grebel 2010; Kuzma et al. 2018) to the chemodynamical identification of former GC stars in the MW

halo field (Martell & Grebel 2010; Koch et al. 2019a; Fernández-Trincado et al. 2019; Tang et al. 2019; Hanke et al. 2020b)

The key signature to identify a bona fide cluster escapee lies in the chemical anomalies inherent in the multiple populations of the GSs (Carretta et al. 2009; Milone et al. 2017; Bastian & Lardo 2018; Gratton et al. 2019). As a result of high-temperature proton-capture reactions in the CNO cycle and its Ne-Na chain in a first generation of massive stars, the second generation that forms from the ejecta of these polluters is found to be rich in He, N, Na, and Al, while depleted in C, O, and Mg, which leads to the characteristic anticorrelations (Na-O, Mg-Al) and bimodalities (e.g., in CN) observed in any given GC (Cohen 1978; Carretta et al. 2009; Hanke et al. 2017; Bastian & Lardo 2018). The remainder of the chemical inventory of the second stellar generation remains largely unaltered by the involved nuclear reactions. These chemical patterns are indeed the best tracers of GC escapees, provided they were part of the second generation, as these characteristic abundances are predominantly found in GCs across the entire mass range, while absent in young open clusters, dwarf galaxies, and in situ halo field stars (Pilachowski et al. 1996; Geisler et al. 2007; Bragaglia et al. 2017; Bekki 2019).

Based on the these chemical signatures, recent quantitative analyses have estimated that about 11% of the stellar MW halo originated from now defunct GCs (Martell & Grebel 2010;

Send offprint requests to: A.J. Koch-Hansen; e-mail: andreas.koch@uni-heidelberg.de

[★] Based on observations obtained at ESO Paranal Observatory, program 0104.D-0059.

Martell et al. 2011; Koch et al. 2019a; Hanke et al. 2020b)¹, an order of magnitude that is bolstered by simulations (e.g., Reina-Campos et al. 2020). Typically, such studies employ low-resolution spectroscopy, which is suitable to determine CN-band strengths, but is not sufficient to perform detailed chemical abundance analyses that inform us about the chemical properties of the progenitor cluster (cf. Ramírez et al. 2012; Lind et al. 2015; Hendricks et al. 2016; Majewski et al. 2017; Fernández-Trincado et al. 2016, 2017). Taking the chemical identification of potentially former GC stars in the halo field one step further, Hanke et al. (2020b) added the kinematic dimensions afforded by the astrometry from the second data release (DR2) of the *Gaia* mission (Lindegren et al. 2018; Gaia Collaboration et al. 2018). This allowed us not only to detect extra-tidal stars around known GCs, but also to trace back stars with common phase-space portions to potentially common progenitors (see also Savino & Posti 2019). In addition to disrupting GCs in the present-day MW halo, we also need to consider the accretion of (dwarf) galaxy satellites. On the one hand, this leads to the donation of their GC systems, thereby increasing the census of the GC population in the Galaxy (Cohen 2004; Forbes & Bridges 2010; Law & Majewski 2010; Carretta et al. 2017; Massari et al. 2019; Myeong et al. 2019; Kruijssen et al. 2019; Koch & Côté 2019; Forbes 2020). On the other hand, the most massive GCs in the MW system are often considered the former nuclei of disrupted dwarf galaxies, leading to broad abundance spreads and pronounced multiple populations that are unequalled in the lower-mass star clusters (Bassino & Muzzio 1995; Sarajedini & Layden 1995; Forbes et al. 2004; Hilker et al. 2004; Kayser et al. 2006; Johnson & Pilachowski 2010). Of these clusters the most massive GC in the MW system, ω Centauri (\equiv NGC 5139; hereafter ω Cen), has long been discussed as the core of a dwarf galaxy satellite (e.g., Lee et al. 1999; Bekki & Freeman 2003; Romano et al. 2007; Valcarce & Catelan 2011); its metallicities show a broad range from -2.5 to -0.8 dex and its chemical abundance inhomogeneities are many (Freeman & Rodgers 1975; Cohen 1981; Suntzeff & Kraft 1996; Hilker et al. 2004; McWilliam & Smecker-Hane 2005; Johnson & Pilachowski 2010; Villanova et al. 2014; Magurno et al. 2019; Johnson et al. 2020).

Based on a large spectroscopic sample from the Radial Velocity Experiment (RAVE; Steinmetz et al. 2006; Kordopatis et al. 2013), Fernández-Trincado et al. (2015) kinematically associated 15 halo stars with ω Cen that were either subject to high-velocity ejections from it some 200 Myr ago or that had had close encounters with this particular GC at high relative velocities. In this work we present a high-resolution, high signal-to-noise (S/N) chemical abundance analysis of one of these candidates, the metal-poor ($[\text{Fe}/\text{H}] \sim -2$ dex) field star J110842.1–715260 (hereafter J110842).² As the relative velocity in the close encounter with ω Cen, at $v_{\text{rel}}=275 \text{ km s}^{-1}$, is rather high, Fernández-Trincado et al. (2015) concluded that it is unlikely that this star (and other similar ones) directly escaped from the GC, rather that it encountered and interacted with the GC between 45 and 290 Myr ago³. The full sample of the RAVE- ω Cen associates

shows chemical abundances that are consistent with the stellar populations of this object; however, the RAVE spectra only allowed the determination of the α -elements Mg, Si, and Ti, and Al and Ni. For J110842 only Al and Ni could be determined. Therefore, a more complete sampling of the abundance space has yet to be conducted, in order to investigate whether the origin of this star is indeed similar to that of ω Cen stars and, if so, whether it classifies as a first- or second-generation star.

This paper is organized as follows. In Sect. 2 we describe the data, followed by details of the abundance analysis in Sect. 3. The resulting chemical abundances are presented in Sect. 4. We discuss the results in the context of ω Cen’s chemodynamical properties in Sect. 5.

2. Data

Star J110842 was observed on the night of March 03, 2020, with the Ultraviolet and Visual Echelle Spectrograph (UVES; Dekker et al. 2000) at the Very Large Telescope (Program 0104.D-0059; P.I. C.J. Hansen). We employed the 390/564 setting with dichroic 1, leading to a broad wavelength coverage of 3285–4518, 4623–5600, and 5672–6647 Å, and a high spectral resolving power of $R \sim 40000$. An exposure time of 2700 seconds yielded a S/N of ~ 50 , 120, and 150 per pixel at 4000, 5200, and 6200 Å. The data were reduced in the standard manner using the ESO UVES reduction workflow recipes (version 6.1.3) that perform bias correction, order tracing, flat fielding, and wavelength calibration using calibration data that were obtained on the same day as the observations.

We measured the star’s radial velocity from a cross-correlation against a template of similar stellar parameters using the Image Reduction and Analysis Facility (IRAF) *fxcor* task. This yielded a heliocentric velocity of $v_{\text{HC}}=273.1 \pm 0.1 \text{ km s}^{-1}$, which agrees well with the values reported from the lower-resolution RAVE and *Gaia* spectra to within 0.4 km s^{-1} (see Table 1).

Table 1. Properties of the target star.

Parameter	Value	Reference
α (J2000.0)	11:08:42.12	1
δ (J2000.0)	−71:52:59.9	1
G	11.117	2
G_{BP}	11.117	2
G_{RP}	10.239	2
L	1224 L_{\odot}	2
v_{HC}	273.1 \pm 0.1 km s^{-1}	3
T_{eff}	4421 \pm 50 K	3
$\log g$	0.61 \pm 0.10	3
ξ	2.19 \pm 0.10 km s^{-1}	3
$[\text{M}/\text{H}]$	−2.10	3
d (<i>Gaia</i>)	4.6 $^{+0.7}_{-0.5}$ kpc	4
μ_{α}	−6.66 \pm 0.05	1
μ_{δ}	0.50 \pm 0.04	1

References. (1): Lindegren et al. (2018); (2): Gaia Collaboration et al. (2018); (3): This work; (4): Bailer-Jones et al. (2018).

¹ This value depends, among other factors, on the adopted fraction of first-generation stars that were lost from the GCs at early times. While Koch et al. (2019a) adopt a fraction of 56%, the recent analysis of Hanke et al. (2020b) assigns larger values of 50–80%, which would raise the inferred halo fraction to the 20% level.

² This star was observed as part of the CERES project (“Chemical Evolution of R-process Elements in Stars”) and thus has the alternate ID CES1108–7153 (C.J. Hansen et al., in prep.).

³ Depending on the adopted Galactic potential. The orbital analysis of Fernández-Trincado et al. (2015) also relied on proper motions from the

UCAC4 (Zacharias et al. 2013), which, however, are in good agreement with the latest *Gaia* values.

3. Chemical abundance analysis

We performed a standard abundance analysis that employed a mixture of equivalent width (EW) measurements, carried out via Gaussian fits with the IRAF *splot* task, and spectrum synthesis. Here we employed the same line list as in Koch & McWilliam (2014, see Table 2) with further additions in the syntheses from Biémont et al. (2000), Den Hartog et al. (2003), Den Hartog et al. (2006), Lawler et al. (2007), Lawler et al. (2008), Lawler et al. (2009), Sneden et al. (2009), and Hansen et al. (2013).

Hyperfine splitting was included where appropriate. The

Table 2. Linelist

λ [Å]	Species	E.P. [eV]	$\log gf$	EW [mÅ]
6300.31	O I	0.00	-9.819	42
6363.79	O I	0.02	-10.303	7
5682.63	Na I	2.10	-0.700	46
5688.20	Na I	2.10	-0.460	66
6154.23	Na I	2.10	-1.560	9
6160.75	Na I	2.10	-1.260	17
4702.99	Mg I	4.35	-0.440	141
5528.42	Mg I	4.35	-0.481	156
5711.09	Mg I	4.33	-1.728	62

Notes. Table 2 is available in its entirety in electronic form via the CDS.

main abundance analysis was carried out using the ATLAS grid of one-dimensional, 72-layer, plane-parallel, line-blanketed Kurucz models without convective overshoot and the α -enhanced opacity distribution functions AODFNEW (Castelli & Kurucz 2003). We further assumed that local thermodynamic equilibrium (LTE) holds for all species. All computations relied on the stellar abundance code MOOG (Sneden 1973, 2014 version) unless noted otherwise.

3.1. Stellar parameters

To derive stellar parameters, we used photometry provided by *Gaia* DR2. We populated the parameter space using computed ATLAS9 model atmosphere grids by Castelli & Kurucz (2003). This contains theoretical values of $G_{BP} - G_{RP}$, A_G , $E(G_{BP} - G_{RP})$, and bolometric corrections for each set of effective temperatures (T_{eff}), surface gravities ($\log g$), and metallicities ($[\text{Fe}/\text{H}]$) in the range of $3500 \leq T_{\text{eff}} \leq 6000$ K, $0 \leq \log g \leq 4$, and $-4 \leq [\text{Fe}/\text{H}] \leq +0.5$. The reddening $E(G_{BP} - G_{RP})$ was computed using the reddening law of Fitzpatrick et al. (2019). In order to determine the best suite of the stellar parameters T_{eff} and $\log g$ for our target star J110842, the following iterative procedure was used:

1. The initial metallicity was estimated via the literature value of -1.6 (Kunder et al. 2017) and T_{eff} was derived by interpolating in $G_{BP} - G_{RP}$;
2. The bolometric correction was derived by interpolation from the new T_{eff} ;
3. $\log g$ was derived using the above bolometric correction and T_{eff} ;
4. A_G and $E(G_{BP} - G_{RP})$ were derived by interpolating in T_{eff} ;
5. G and $G_{BP} - G_{RP}$ were de-reddened using the reddening maps by Schlafly & Finkbeiner (2011, $A_V=0.81$);
6. The procedure was iterated until the difference in temperature between successive runs was less than 50 K.

The microturbulence velocities (ξ) in each step were estimated using the calibration of Mashonkina et al. (2017). Here

we note that the final value of 2.19 km s^{-1} provides an excellent balance in the plot of line-by-line abundances with equivalent widths of the Fe I lines.

The final photometric parameter set of $T_{\text{eff}}=4421$ K and $\log g=0.61$ dex yields an iron abundance from the neutral and ionized species of $[\text{Fe I}/\text{H}]=-1.84$ and $[\text{Fe II}/\text{H}]=-2.10$ dex, respectively. Thus, there is a pronounced ionization imbalance seen in this star when employing the photometrically derived surface gravity. Moreover, no equilibrium of the Fe I abundance with excitation potential could be reached upon using the photometric temperature. This is a well-known problem for stars more metal poor than about -1.5 dex, as has been systematically evaluated by Mucciarelli & Bonifacio (2020). The suggested reasons for these discrepancies are the commonly used assumptions in the spectroscopic approach, to wit, LTE and/or the one-dimensional treatment of the atmospheres. Therefore, following the recommendation of Mucciarelli & Bonifacio (2020), we adopt in the following the stellar parameters derived photometrically above and we continue by choosing the Fe abundance from the ionized species as the metallicity scale of star J110842.

3.2. Abundance errors

The statistical errors on our abundance ratios were determined via the standard deviation and the number of measured lines per element used to derive its abundance. Furthermore, we performed a systematic error analysis by varying each stellar parameter about its respective uncertainty: $T_{\text{eff}} \pm 50$ K, $\log g \pm 0.1$ dex, $[\text{M}/\text{H}] \pm 0.1$ dex, and $\xi \pm 0.1 \text{ km s}^{-1}$. We further ran the identical analyses as above using solar-scaled opacity distributions (ODFNEW) and take one-quarter of the ensuing deviation to mimic an ignorance of the α -enhancement in the star of 0.1 dex. The respective deviations of the abundance ratios from the bona fide results from the unaltered atmospheres are listed in Table 3; a conservative upper limit to the total systematic uncertainty in terms of the squared sum of all contributions is given in the last column, although strong correlations between the impacts from the various atmospheric parameters can be expected (see, e.g., McWilliam et al. 1995; Hanke et al. 2020a).

4. Results

All abundance results and the errors as described above are listed in Table 4. These values adopt the solar abundance scale of Asplund et al. (2009). In the following figures we place our results into context with the MW halo, bulge, and disks, and ω Cen. For ω Cen we used the data of Johnson & Pilachowski (2010) and Simpson et al. (2020), who chemodynamically extracted cluster candidates from the GALAH survey (De Silva et al. 2015). Here we also show the abundance ratios of those stars. Figures 1, 3, and 4 show the abundance comparison, where we restrict ourselves to those elements in common between our study and that of ω Cen. The remaining elements, though not explicitly shown, are discussed individually below.

4.1. Metallicity

At $[\text{Fe II}/\text{H}]=-2.10$ dex, J110842 samples the metal-poor tail of ω Cen's metallicity distribution (Fig. 1, top). This distribution has long been known to show a large dispersion and covers a range of more than 1.7 dex (Johnson & Pilachowski 2010). As this object is commonly considered the nucleus of a formerly more massive dwarf galaxy, such a large spread and the occurrence of

Table 3. Systematic error analysis.

Species	T_{eff} ± 50 K	$\log g$ ± 0.1 dex	$[M/H]$ ± 0.1 dex	ξ ± 0.1 km s $^{-1}$	ODF	Sys.
CH (G-band)	± 0.03	∓ 0.03	∓ 0.07	∓ 0.01	-0.08	0.08
O I	± 0.02	± 0.04	± 0.03	∓ 0.01	-0.08	0.07
Na I	± 0.05	∓ 0.02	∓ 0.01	∓ 0.01	0.04	0.06
Mg I	± 0.06	∓ 0.03	∓ 0.02	∓ 0.04	0.05	0.08
Si I	± 0.02	± 0.01	∓ 0.01	∓ 0.01	0.01	0.03
Ca I	± 0.07	∓ 0.02	∓ 0.02	∓ 0.04	0.05	0.09
Sc II	∓ 0.01	± 0.03	± 0.02	∓ 0.03	-0.06	0.06
Ti I	± 0.14	∓ 0.02	∓ 0.03	∓ 0.06	-0.03	0.16
Ti II	∓ 0.01	± 0.03	± 0.02	∓ 0.04	-0.05	0.06
V I	± 0.11	∓ 0.02	∓ 0.02	∓ 0.01	0.03	0.12
Cr I	± 0.12	∓ 0.02	∓ 0.03	∓ 0.05	0.02	0.14
Mn I	± 0.11	∓ 0.03	∓ 0.03	∓ 0.03	0.05	0.12
Fe I	± 0.08	∓ 0.02	∓ 0.02	∓ 0.05	0.04	0.10
Fe II	∓ 0.04	± 0.04	± 0.02	∓ 0.02	-0.06	0.07
Co I	± 0.09	∓ 0.02	∓ 0.02	∓ 0.04	0.05	0.11
Ni I	± 0.06	∓ 0.01	∓ 0.01	∓ 0.02	0.04	0.09
Cu I	± 0.08	∓ 0.01	∓ 0.01	∓ 0.02	0.04	0.09
Zn I	∓ 0.03	± 0.01	± 0.01	∓ 0.03	-0.01	0.05
Sr II	± 0.01	± 0.01	± 0.02	∓ 0.01	-0.05	0.03
Y II	∓ 0.01	± 0.03	± 0.02	∓ 0.04	-0.05	0.06
Zr II	∓ 0.01	± 0.03	± 0.02	∓ 0.01	-0.05	0.05
Ba II	± 0.03	± 0.04	± 0.02	∓ 0.08	-0.09	0.11
La II	± 0.02	± 0.02	± 0.01	∓ 0.04	-0.03	0.05
Ce II	± 0.01	± 0.03	± 0.02	∓ 0.01	-0.06	0.05
Pr II	± 0.02	± 0.03	± 0.02	∓ 0.01	-0.07	0.06
Nd II	± 0.01	± 0.02	± 0.01	∓ 0.03	-0.03	0.04
Sm II	± 0.02	± 0.03	± 0.02	∓ 0.01	-0.05	0.05
Eu II	± 0.02	± 0.02	± 0.02	∓ 0.07	-0.06	0.08
Gd II	± 0.01	± 0.02	± 0.01	∓ 0.01	-0.04	0.03
Dy II	± 0.02	± 0.02	± 0.01	∓ 0.02	-0.04	0.04
Hf II	± 0.05	± 0.05	± 0.05	∓ 0.03	-0.02	0.09
Pb II	± 0.10	∓ 0.02	∓ 0.07	∓ 0.01	0.10	0.13

Table 4. Abundance results. Abundance ratios for ionized species are given relative to Fe II. For iron itself, $[\text{Fe}/\text{H}]$ is listed. The line-to-line scatter, σ , and number of measured lines, N , indicate the statistical error.

Species	$[\text{X}/\text{Fe}]$	σ	N	Species	$[\text{X}/\text{Fe}]$	σ	N	Species	$[\text{X}/\text{Fe}]$	σ	N
CH (G-band)	-0.85	...	1 ^S	Mn I	-0.50	0.12	9 ^H	La II	0.40	0.09	6 ^H
O I	0.65	0.28	2 ^S	Fe I	-1.91	0.13	78	Ce II	0.13	0.07	3 ^S
Na I	0.51	0.05	4	Fe II	-2.01	0.05	8	Pr II	0.32	0.07	5 ^S
Mg I	0.54	0.14	3	Co I	0.15	0.15	5 ^H	Nd II	0.19	0.09	5 ^S
Si I	0.48	0.06	2	Ni I	-0.03	0.10	15	Sm II	0.24	0.07	3 ^S
Ca I	0.31	0.20	15	Cu I	-0.33	0.10	2	Eu II	0.00	...	1 ^S
Sc II	0.11	0.14	2 ^H	Zn I	0.13	0.08	2	Gd II	0.15	...	1 ^S
Ti I	0.29	0.12	11	Sr II	<0.30	...	1 ^S	Dy II	0.23	0.13	3 ^S
Ti II	0.38	0.15	10	Y II	0.10	0.08	5	Er II	-0.02	...	1 ^S
V I	0.13	0.03	6	Zr II	0.36	...	1	Hf II	-0.05	...	1 ^S
Cr I	-0.06	0.07	7	Ba II	0.23	0.01	3 ^H	Pb I	0.60	...	1 ^S

Notes. “H” indicates that hyperfine structure was accounted for; “S” denotes abundances that were derived from spectrum synthesis.

very metal-poor stars down to -2.5 dex (Johnson et al. 2020) is not surprising as this is seen in many dwarf spheroidal galaxies in the Local Group (e.g., Koch 2009).

4.2. Light elements: C, N, O, Na

Fernández-Trincado et al. (2015) noted that ωCen is special in that it covers a broad range in all of their analyzed abundance patterns to the point that it overlaps with all MW components. They concluded that any similarity in these properties is “not very useful” to constrain the origin of the stars. However, their element abundances, drawn from the RAVE survey, were only

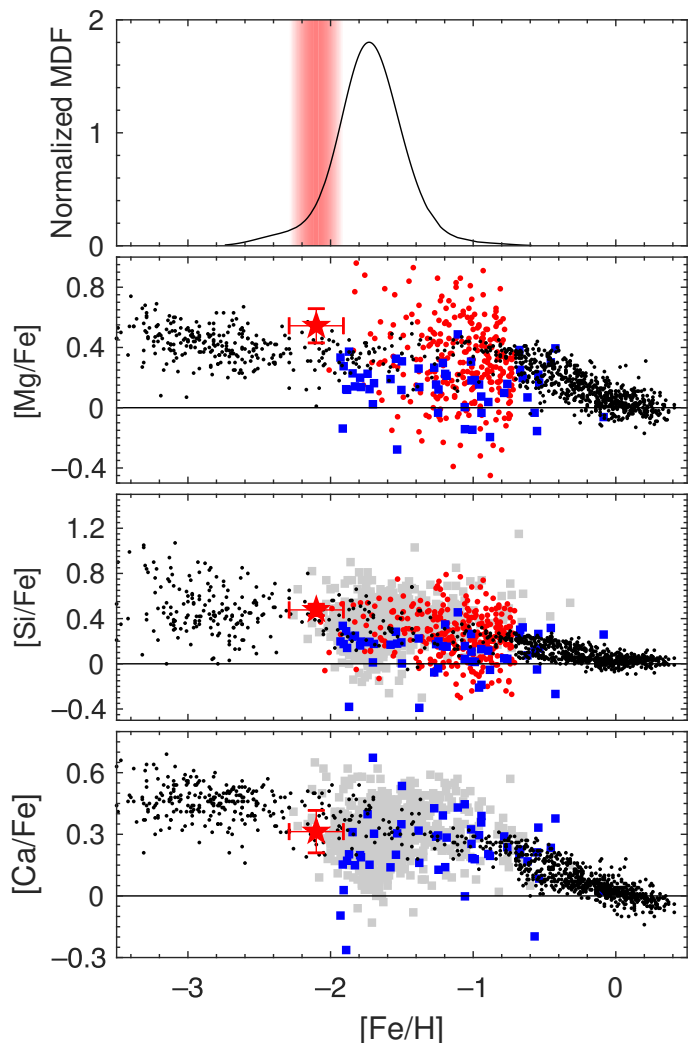


Fig. 1. Chemical abundances of J110842 (red star) in comparison with ω Cen (gray squares: Johnson & Pilachowski 2010; blue squares: Simpson et al. 2020) and the MW halo (Roederer et al. 2014) and disks (Bensby et al. 2014), shown as black dots. The 329 candidate ω Cen associates from Fernández-Trincado et al. (2015) are indicated as red points. The error bar accounts for statistical and systematic uncertainties. The top panel shows the error-weighted metallicity distribution from Johnson et al. (2020), on which is highlighted the 1σ error range of the metallicity determined in the present work.

limited to Fe, Al, and Ni⁴. Therefore, we highlight here some of the elements that provide a greater clue to any potential origin of J110842.

One of the characteristics of GCs is the presence of multiple stellar generations and the ensuing light-element variations as a result of p -capture reactions in an early generation of stars (Kayser et al. 2008; Carretta et al. 2009; Bastian & Lardo 2018). These variations include bimodalities in CN and associated anticorrelations with CH strength. We measured the strength of the commonly used CH and CN bands using the index definitions of Norris et al. (1981), which was then translated into a $\delta S(3839)$ index to remove dependencies on evolutionary status (Martell & Grebel 2010; Koch et al. 2019a). The main uncertainty in this

⁴ Abundances for the other α -elements (Mg, Si, Ti) were reported for the remainder of the ω Cen candidates in Fernández-Trincado et al. (2015), but had not been derived for star J110842.

quantity is the required absolute magnitude of the star, which relies on its distance that still shows large errors (see Table 1). At $\delta S(3839)=0.253$, J110842 qualifies as a CN-strong star (see, e.g., Fig. 5 in Koch et al. 2019a). As such it would be tempting to characterize it as a second-generation star, bolstering its origin in a GC-like environment, which also requires it to be CH-weak. We measured an S(CH) index of 0.819, and combined with the lower [C/Fe] we conclude that this instead argues in favor of a C-normal star (e.g., Kirby et al. 2015; Koch et al. 2019b), with values that are appropriate for its luminosity of $1224 L_{\odot}$ (Gaia Collaboration et al. 2018).

Similarly, genuine GCs are infamous for having a pronounced Na-O anticorrelation, which is also prominently seen in ω Cen (Norris & Da Costa 1995b; Gratton et al. 2011; Simpson et al. 2020) and particularly extended below -1.3 dex (Marino et al. 2011). In Fig. 2 we show our Na and O measurements for J110842 superimposed on the literature data from the above sources.

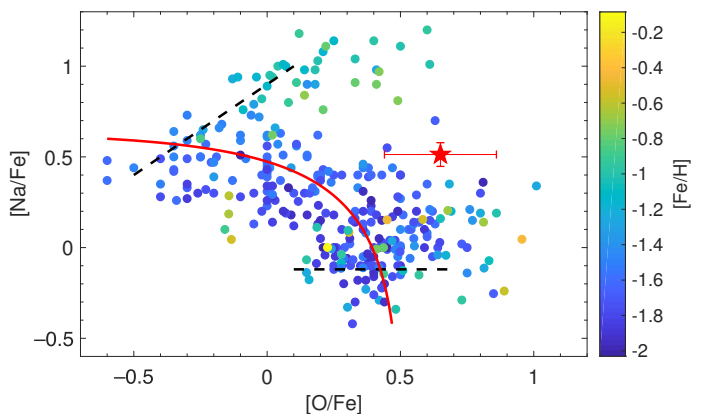


Fig. 2. Sodium-oxygen anticorrelation using data from Marino et al. (2011) and Simpson et al. (2020), color-coded by metallicity. Star J110842 is indicated by a red star. We also indicate the empirical separations into first, second, and extreme generations (dashed black) and the simplistic dilution model (red line) by Carretta et al. (2009).

While the value of [O/Fe] for J110842 at 0.65 dex is compatible with that of a metal-poor, α -enhanced halo star, the [Na/Fe] value of 0.55 dex is rather high and makes this star fall into the regime of Na-strong second-generation GC stars. We note that all our abundances have been derived in an LTE framework. However, interpolating the grid of non-LTE (NLTE) corrections by Lind et al. (2011) yields a departure from the LTE abundance of ~ -0.06 dex, while the correction for oxygen is null for the parameters similar to our star (Sitnova et al. 2013). Thus, even if NLTE corrections are accounted for, we cannot exclude a second-generation origin for this star based on its Na abundance, and marginally supported by its O abundance and CN strength.

Finally, we note that GCs often show strong variations in Al that mildly correlate with Mg, owing to the hot branches of proton-burning. However, the spectral range of our UVES setting did not allow us to determine an Al abundance from the 6696 Å line. Conversely, the blue line at 3961 Å lies in the wing of the strong Ca H line, making a meaningful abundance determination difficult. Instead, we use the value of Fernández-Trincado et al. (2015) for further discussion. Considering the higher Mg and O abundances in our star, their adopted [Al/Fe] of 0.38 dex lies at the low branch of Al abundances, which is consistent with an association with a second stellar population in a GC (e.g., Carretta et al. 2013).

4.3. α -elements: Mg, Si, Ca, Ti

The α -elements in J110842 present few surprises. At an $[\alpha/\text{Fe}]$ value of 0.42 ± 0.03 dex it falls square on the α -plateau delineated by metal-poor halo stars and the bulk of ωCen 's broad abundance space (Figs. 1,3). This indicates enrichment via standard nucleosynthesis in supernovae of type II (SNe II) and does not allow us to further investigate the question of a peculiar origin of this star based on these chemical tracers.

4.4. Fe-peak elements: Sc, V, Cr, Mn, Co, Ni, Cu

As is true for the α -elements, the Fe-peak elements also follow the trends outlined by metal-poor halo and ωCen stars (see Figures 3,4, and also Cohen 1981; Norris & Da Costa 1995a; Smith et al. 1995; Pancino et al. 2011; Magurno et al. 2019 for ωCen) and that are mainly set by SN Ia nucleosynthesis (e.g., Kobayashi et al. 2006).

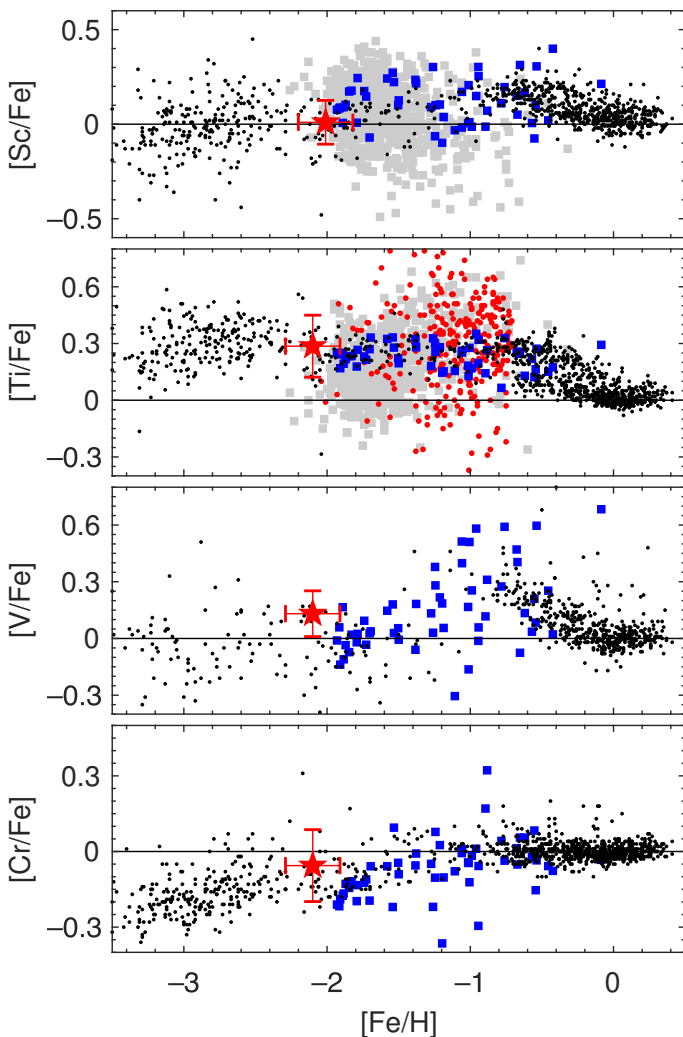


Fig. 3. Same as Fig. 1, but for the lighter Fe-peak elements. Disk values for Sc and V are from Battistini & Bensby (2015).

Copper (bottom panel of Fig. 4), in contrast, has been a matter of high interest in this GC, and Cunha et al. (2002) noted that Cu stays approximately constant and remains below the trend seen in halo stars over a broad metallicity range of ~ -2 to -0.8 dex. This was thought as being due to a lower-level contribution

of SNe Ia to the chemical evolution in that metallicity range. Furthermore, by chemical similarity to the Sagittarius dwarf galaxy, McWilliam & Smecker-Hane (2005) lend support to the notion that ωCen is rather the nucleus of a former, more massive system. The target of this study, J110842, overlaps with the metal-poor halo and the metal-poor tail of the ωCen distribution. Our own values and the cited literature values were derived under the assumption of LTE. It appears that the Cu abundances are affected by NLTE effects (Andrievsky et al. 2018; Shi et al. 2018), although different model-atoms and NLTE codes provide different results, especially at low metallicity. This notion is reinforced by the observed deviation between Cu I and Cu II abundances observed by Roederer & Barklem (2018). Bonifacio et al. (2010) found strong granulation effects on the resonance lines (although not used here); however, the combined effect of granulation and NLTE effects still needs to be investigated. It would therefore be interesting to reinvestigate the Cu abundances in ωCen , and in J110842, using a more sophisticated modeling.

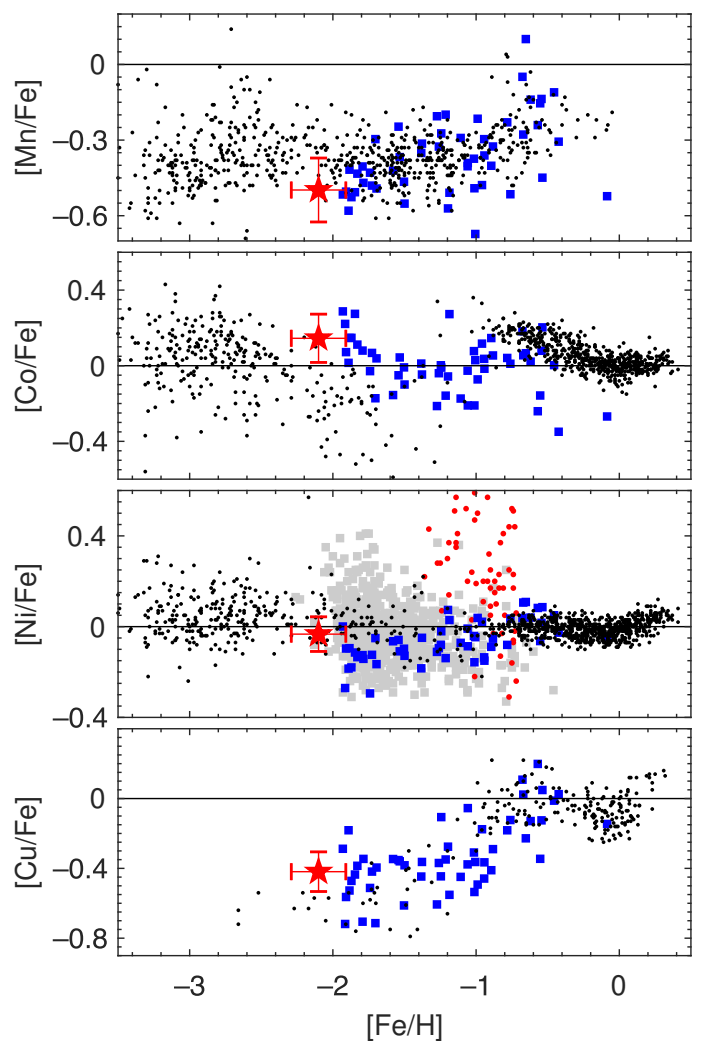


Fig. 4. Same as Fig. 1, but for the remaining Fe-peak elements. Abundances for Mn are from Sobeck et al. (2006), Co data are from Battistini & Bensby (2015), and Cu for the MW disks and halo are from Mishenina et al. (2002, 2011).

We can also use our measurements to address the broader context of Galactic chemical evolution. Here Hawkins et al. (2015) posited that the $[\text{Mg}/\text{Mn}]$ versus $[\text{Al}/\text{Fe}]$ plane is a pow-

erful indicator for an origin in major, dwarf-galaxy-like accretion events versus in situ formed stars that are enhanced in the α -elements. In J110842 we measured a very high value for $[\text{Mg}/\text{Mn}]$ of 1.04 ± 0.09 dex. If we had taken into account NLTE effects, this overabundance would be even larger (Bergemann et al. 2019). In order to qualify as an accreted object, the $[\text{Al}/\text{Fe}]$ abundance in J110842 would need to be subsolar at its Mg and Mn abundances, according to the distinctive line in Horta et al. (2020). However, since Fernández-Trincado et al. (2015) reported on a higher $[\text{Al}/\text{Fe}]$ of 0.38 dex, this instead argues for an in situ formation or that the birth environment has chemically evolved.

4.5. *n*-capture elements: Zn, Sr, Y, Zr, Ba, La, Ce, Pr, Nd, Sm, Eu, Gd, Dy, Er, Hf, Pb

Our abundance results for the selected heavy elements overlapping with the literature for ω Cen are shown in Fig. 5. In addition, the values for J110842 for these elements are in close agreement with metal-poor halo stars and the metal-poor end of the GC abundance distribution, indicating that the same nucleosynthetic processes were at play.

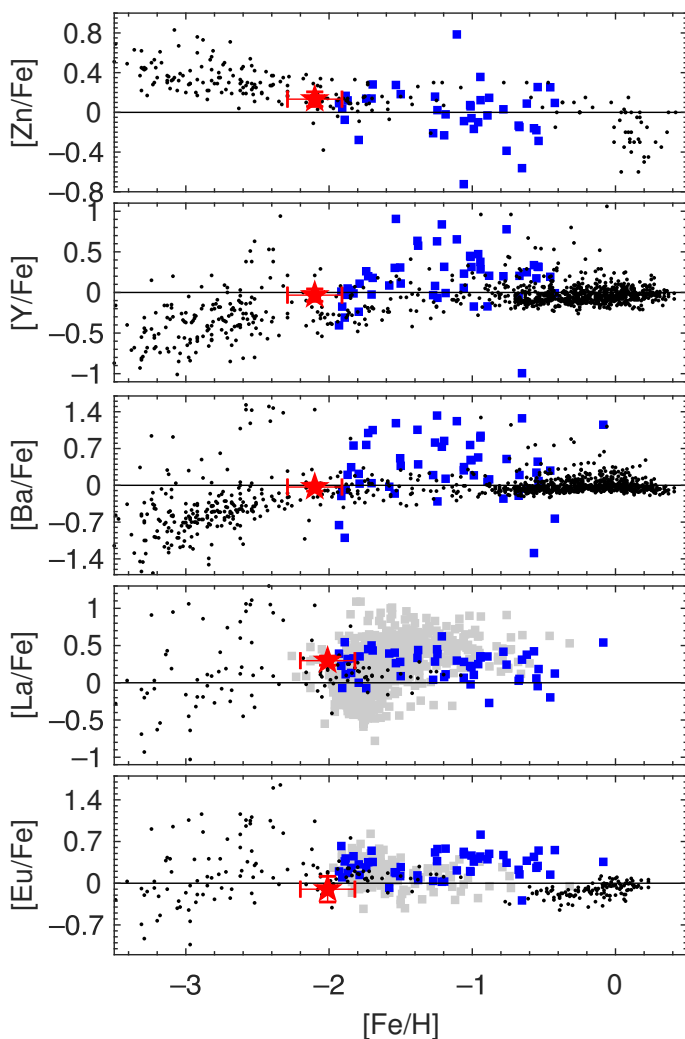


Fig. 5. Same as Fig. 1, but for the neutron-capture elements ($Z \geq 30$). The reference MW abundances are from Barbuy et al. (2015) for Zn, and from Koch & Edvardsson (2002) for Eu.

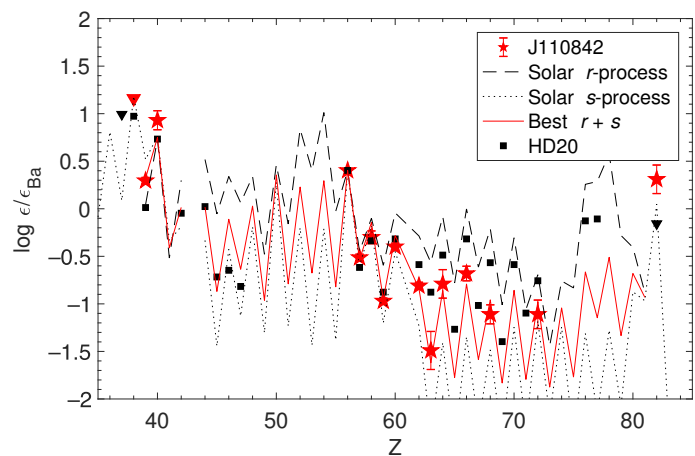


Fig. 6. Abundance distribution of the heavy elements, normalized to Ba. Also shown are the solar *s*- and *r*-process contributions (Burriss et al. 2000) and the best-fit linear combination of the contributions. Finally, we overplot the *r*-process benchmark star HD 20 as black squares (Hanke et al. 2020a).

Among the neutron-capture elements we particularly note the *s*-process elements Y, Ba, and La (middle three panels of Fig. 5). Dating back to Lloyd Evans (1983), a bimodal behavior has now been established; for instance, from their high-resolution analysis of 113 RR Lyr stars in ω Cen Magurno et al. (2019) reported solar $[\text{Y}/\text{Fe}]$ values for stars more metal poor than approximately -1.5 dex, while the more metal-rich component showed enhanced element abundances. This is also seen in terms of a significantly larger scatter above that metallicity cut in the data of Simpson et al. (2020), among others. Furthermore, the values for $[\text{La}/\text{Fe}]$ found by Johnson & Pilachowski (2010) also show a clear bimodality. This has been interpreted in terms of markedly different stellar populations, where the more metal-rich component was (self-)enriched over a long timescale by low-mass asymptotic giant branch stars (e.g., Norris & Da Costa 1995a; Smith et al. 2000; Cunha et al. 2002), while the sudden increase in the abundance ratios with $[\text{Fe}/\text{H}]$ is compatible with ω Cen being the remnant of a more massive dwarf galaxy (Romano et al. 2007; Magurno et al. 2019). The solar value of $[\text{Y}/\text{Fe}]$ in J110842 at its low metallicity and its solar $[\text{Ba}/\text{Fe}]$ are fully compatible with the lower-metallicity component.

Figure 6 shows the overall abundance distribution of heavy ($Z > 30$) elements we were able to measure in J110842. Here we note that Sr in its spectrum shows very strong resonance lines (at 4077 and 4215 Å) that are likely saturated. Therefore, we were only able to place a limit of ~ 0.3 dex on the $[\text{Sr}/\text{Fe}]$ value. As noted before, J110842 is mainly characterized by standard nucleosynthesis and the majority of elements lie between the (solar) *s*- and *r*-process distributions, as is expected if we consider, at this metallicity, that AGB stars have already started to contribute some *s*-process material to the Galactic chemical evolution (e.g., Simmerer et al. 2004). A χ^2 fit indicates that J110842 has received an admixture of *s*-process elements at the 60% level. Another assessment of the *r*- and *s*-process contributions can be made in comparison to the cleaner *r*-process tracer HD 20 (black symbols in Fig. 6), which at a metallicity that is lower than the Sun's displays a very clean *r*-process pattern. However, in this direct comparison J110842 also comes out as a *r*-*s* mixed star with not just one main polluter governing its formation. A further characterization of the donors to the chemical enrichment of this star, such as SNe or AGB stars, cannot be unambiguously

made in stars like J110842, where the effects of mixing and dilution need to be properly dealt with (Magg et al. 2020; Hansen et al. 2020).

5. Discussion

In our endeavor to find signs of a chemical association of the halo star J110842 with the massive GC ω Cen, as has been previously suggested from their relative dynamics, we performed an extensive chemical abundance study. We showed that the majority of the heavier elements ($Z \geq 12$) is fully compatible with those seen in ω Cen. This is, however, not surprising given the large overlap of the GC abundance space with that of metal-poor halo field stars at this metallicity (-2.1 dex), and cannot unambiguously argue for a GC origin of J110842. Here it is more interesting to look at the light elements. The high Na abundance and its characterization as a CN-strong star indeed lend support to the hypothesis that it is a former second-generation GC star, while the enhancement in O and its CH-normal nature appear to mitigate this.

Fernández-Trincado et al. (2015) argued that it is unlikely that stars with high relative encounter speeds have been ejected from ω Cen, but just had chance encounters when their orbits coincided. The central escape velocity of the GC is on the order of $60\text{--}100\text{ km s}^{-1}$ (Gnedin et al. 2002; Gao et al. 2015), which compares to the computed encounter velocity with J110842 in excess of 200 km s^{-1} . On the other hand, extreme horizontal branch stars at high tangential motions of up to $90\text{--}310\text{ km s}^{-1}$ have been found in ω Cen, and they are most likely to escape the GC within the next Myr or so (Gao et al. 2015), in which case a former origin of our target star within the GC remains plausible. Here we note that Lind et al. (2015) associate a halo star with typical GC signatures such as enhanced Al and low Mg abundances with having escaped from ω Cen at high speed. Such high-speed ejections ($>100\text{ km s}^{-1}$) are suggested if interactions with binaries or black holes are evoked (Gvaramadze et al. 2009; Lützgendorf et al. 2012).

As to the origin of ω Cen itself, Myeong et al. (2019) have associated it with the recently discovered massive Sequoia accretion event, while Ibata et al. (2019) paired it with the Fimbulthul stream. The latter poses an intriguing parallel to our star as its abundance distribution is very similar to the most metal-poor stream candidate analyzed by Simpson et al. (2020). This emphasizes the power of chemical tagging in meaningfully investigating the manifold of eclectic GC-stream-halo-field interfaces.

Acknowledgements. The authors thank the anonymous referee for a swift and constructive report. AJKH gratefully acknowledges funding by the Deutsche Forschungsgemeinschaft (DFG, German Research Foundation) – Project-ID 138713538 – SFB 881 (“The Milky Way System”), subprojects A03, A05, A11. CJH acknowledges support from the Max Planck Society and from the ChETEC COST Action (CA16117), supported by COST (European Cooperation in Science and Technology). LL, PB and EC gratefully acknowledge support from the French National Research Agency (ANR) funded project “Pristine” (ANR-18-CE31-0017). This work has made use of data from the European Space Agency (ESA) mission *Gaia* (<https://www.cosmos.esa.int/gaia>), processed by the *Gaia* Data Processing and Analysis Consortium (DPAC, <https://www.cosmos.esa.int/web/gaia/dpac/consortium>). Funding for the DPAC has been provided by national institutions, in particular the institutions participating in the *Gaia* Multilateral Agreement. This research made use of atomic data from the INSPECT database, version 1.0 (www.inspect-stars.com).

References

Andrievsky, S., Bonifacio, P., Caffau, E., et al. 2018, MNRAS, 473, 3377

- Asplund, M., Grevesse, N., Sauval, A. J., & Scott, P. 2009, ARA&A, 47, 481
- Bailer-Jones, C. A. L., Ryzbizki, J., Fouesneau, M., Mantelet, G., & Andrae, R. 2018, AJ, 156, 58
- Barbuy, B., Friaça, A. C. S., da Silveira, C. R., et al. 2015, A&A, 580, A40
- Bassino, L. P. & Muzzio, J. C. 1995, The Observatory, 115, 256
- Bastian, N. & Lardo, C. 2018, ARA&A, 56, 83
- Battistini, C. & Bensby, T. 2015, A&A, 577, A9
- Bekki, K. & Freeman, K. C. 2003, MNRAS, 346, L11
- Bekki, K. 2019, MNRAS, 490, 4007
- Bensby, T., Feltzing, S., & Oey, M. S. 2014, A&A, 562, A71
- Bergemann, M., Gallagher, A. J., Eitner, P., et al. 2019, A&A, 631, A80
- Biémont, E., Garnir, H. P., Palmeri, P., Li, Z. S., & Svanberg, S. 2000, MNRAS, 312, 116
- Bonifacio, P., Caffau, E., & Ludwig, H. G. 2010, A&A, 524, A96
- Bragaglia, A., Carretta, E., D’Orazi, V., et al. 2017, A&A, 607, A44
- Bullock, J. S. & Johnston, K. V. 2005, ApJ, 635, 931
- Burris, D. L., Pilachowski, C. A., Armand roff, T. E., et al. 2000, ApJ, 544, 302
- Carretta, E., Bragaglia, A., Gratton, R., & Lucatello, S. 2009, A&A, 505, 139
- Carretta, E., Gratton, R. G., Bragaglia, A., D’Orazi, V., & Lucatello, S. 2013, A&A, 550, A34
- Carretta, E., Bragaglia, A., Lucatello, S., et al. 2017, A&A, 600, A118
- Castelli, F. & Kurucz, R. L. 2003, in IAU Symposium, Vol. 210, Modelling of Stellar Atmospheres, ed. N. Piskunov, W. W. Weiss, & D. F. Gray, A20
- Cohen, J. G. 1978, ApJ, 223, 487
- Cohen, J. G. 1981, ApJ, 247, 869
- Cohen, J. G. 2004, AJ, 127, 1545
- Cooper, A. P., D’Souza, R., Kauffmann, G., et al. 2013, MNRAS, 434, 3348
- Cunha, K., Smith, V. V., Suntzeff, N. B., et al. 2002, AJ, 124, 379
- De Silva, G. M., Freeman, K. C., Bland-Hawthorn, J., et al. 2015, MNRAS, 449, 2604
- Dekel, A. & Silk, J. 1986, ApJ, 303, 39
- Dekker, H., D’Odorico, S., Kaufer, A., Delabre, B., & Kotzlowski, H. 2000, in Society of Photo-Optical Instrumentation Engineers (SPIE) Conference Series, Vol. 4008, Optical and IR Telescope Instrumentation and Detectors, ed. M. Iye & A. F. Moorwood, 534–545
- Den Hartog, E. A., Lawler, J. E., Sneden, C., & Cowan, J. J. 2003, ApJS, 148, 543
- Den Hartog, E. A., Lawler, J. E., Sneden, C., & Cowan, J. J. 2006, ApJS, 167, 292
- Eggen, O. J., Lynden-Bell, D., & Sandage, A. R. 1962, ApJ, 136, 748
- Fernández-Trincado, J. G., Robin, A. C., Vieira, K., et al. 2015, A&A, 583, A76
- Fernández-Trincado, J. G., Robin, A. C., Moreno, E., et al. 2016, ApJ, 833, 132
- Fernández-Trincado, J. G., Zamora, O., García-Hernández, D. A., et al. 2017, ApJ, 846, L2
- Fernández-Trincado, J. G., Beers, T. C., Tang, B., et al. 2019, MNRAS, 488, 2864
- Fitzpatrick, E. L., Massa, D., Gordon, K. D., Bohlin, R., & Clayton, G. C. 2019, ApJ, 886, 108
- Forbes, D. A., Strader, J., & Brodie, J. P. 2004, AJ, 127, 3394
- Forbes, D. A. & Bridges, T. 2010, MNRAS, 404, 1203
- Forbes, D. A. 2020, MNRAS, 493, 847
- Freeman, K. C. & Rodgers, A. W. 1975, ApJ, 201, L71
- Gaia Collaboration, Brown, A. G. A., Vallenari, A., et al. 2018, A&A, 616, A1
- Gao, X.-H., Xu, S.-K., & Chen, L. 2015, Research in Astronomy and Astrophysics, 15, 1639
- Geisler, D., Wallerstein, G., Smith, V. V., & Casetti-Dinescu, D. I. 2007, PASP, 119, 939
- Gnedin, O. Y., Zhao, H., Pringle, J. E., et al. 2002, ApJ, 568, L23
- Gratton, R. G., Johnson, C. I., Lucatello, S., D’Orazi, V., & Pilachowski, C. 2011, A&A, 534, A72
- Gratton, R., Bragaglia, A., Carretta, E., et al. 2019, A&A Rev., 27, 8
- Gvaramadze, V. V., Gualandris, A., & Portegies Zwart, S. 2009, MNRAS, 396, 570
- Hanke, M., Koch, A., Hansen, C. J., & McWilliam, A. 2017, A&A, 599, A97
- Hanke, M., Hansen, C. J., Ludwig, H.-G., et al. 2020a, A&A, 635, A104
- Hanke, M., Koch, A., Prudil, Z., Grebel, E. K., & Bastian, U. 2020b, A&A, 637, A98
- Hansen, C. J., Bergemann, M., Cescutti, G., et al. 2013, A&A, 551, A57
- Hansen, C. J., Koch, A., Mashonkina, L., et al. 2020, A&A, 643, 49
- Hawkins, K., Kordopatis, G., Gilmore, G., et al. 2015, MNRAS, 447, 2046
- Hendricks, B., Boeche, C., Johnson, C. I., et al. 2016, A&A, 585, A86
- Hilker, M., Kayser, A., Richtler, T., & Willemsen, P. 2004, A&A, 422, L9
- Horta, D., Schiavon, R. P., Mackereth, J. T., et al. 2020, arXiv e-prints, arXiv:2007.10374
- Ibata, R. A., Bellazzini, M., Malhan, K., Martin, N., & Bianchini, P. 2019, Nature Astronomy, 3, 667
- Johnson, C. I. & Pilachowski, C. A. 2010, ApJ, 722, 1373
- Johnson, C. I., Dupree, A. K., Mateo, M., et al. 2020, AJ, 159, 254
- Jordi, K. & Grebel, E. K. 2010, A&A, 522, A71
- Kayser, A., Hilker, M., Richtler, T., & Willemsen, P. G. 2006, A&A, 458, 777

- Kaysers, A., Hilker, M., Grebel, E. K., & Willemsen, P. G. 2008, *A&A*, 486, 437
- Kirby, E. N., Guo, M., Zhang, A. J., et al. 2015, *ApJ*, 801, 125
- Kobayashi, C., Umeda, H., Nomoto, K., Tominaga, N., & Ohkubo, T. 2006, *ApJ*, 653, 1145
- Koch, A. & Edvardsson, B. 2002, *A&A*, 381, 500
- Koch, A. 2009, *Astronomische Nachrichten*, 330, 675
- Koch, A. & McWilliam, A. 2014, *A&A*, 565, A23
- Koch, A. & Côté, P. 2019, *A&A*, 632, A55
- Koch, A., Grebel, E. K., & Martell, S. L. 2019a, *A&A*, 625, A75
- Koch, A., Xi, S., & Rich, R. 2019b, *A&A*, 627, A70
- Kordopatis, G., Gilmore, G., Steinmetz, M., et al. 2013, *AJ*, 146, 134
- Kruijssen, J. M. D., Pfeffer, J. L., Reina-Campos, M., Crain, R. A., & Bastian, N. 2019, *MNRAS*, 486, 3180
- Kunder, A., Kordopatis, G., Steinmetz, M., et al. 2017, *AJ*, 153, 75
- Kuzma, P. B., Da Costa, G. S., & Mackey, A. D. 2018, *MNRAS*, 473, 2881
- Law, D. R. & Majewski, S. R. 2010, *ApJ*, 718, 1128
- Lawler, J. E., den Hartog, E. A., Labby, Z. E., et al. 2007, *ApJS*, 169, 120
- Lawler, J. E., Sneden, C., Cowan, J. J., Ivans, I. I., & Den Hartog, E. A. 2009, *ApJS*, 182, 51
- Lawler, J. E., Sneden, C., Cowan, J. J., et al. 2008, *ApJS*, 178, 71
- Lee, Y. W., Joo, J. M., Sohn, Y. J., et al. 1999, *Nature*, 402, 55
- Lee, K. H., Lee, H. M., Fahlman, G. G., & Sung, H. 2004, *AJ*, 128, 2838
- Lind, K., Asplund, M., Barklem, P. S., & Belyaev, A. K. 2011, *A&A*, 528, A103
- Lind, K., Kozlov, S. E., Battistini, C., et al. 2015, *A&A*, 575, L12
- Lindgren, L., Hernández, J., Bombrun, A., et al. 2018, *A&A*, 616, A2
- Lloyd Evans, T. 1983, *MNRAS*, 204, 975
- Lützgendorf, N., Gualandris, A., Kissler-Patig, M., et al. 2012, *A&A*, 543, A82
- Magg, M., Nordlander, T., Glover, S. C. O., et al. 2020, *MNRAS*, 498, 3703
- Magurno, D., Sneden, C., Bono, G., et al. 2019, *ApJ*, 881, 104
- Majewski, S. R., Schiavon, R. P., Frinchaboy, P. M., et al. 2017, *AJ*, 154, 94
- Marino, A. F., Milone, A. P., Piotto, G., et al. 2011, *ApJ*, 731, 64
- Martell, S. L. & Grebel, E. K. 2010, *A&A*, 519, A14
- Martell, S. L., Smolinski, J. P., Beers, T. C., & Grebel, E. K. 2011, *A&A*, 534, A136
- Mashonkina, L., Jablonka, P., Pakhomov, Y., Sitnova, T., & North, P. 2017, *A&A*, 604, A129
- Massari, D., Koppelman, H. H., & Helmi, A. 2019, *A&A*, 630, L4
- McWilliam, A., Preston, G. W., Sneden, C., & Searle, L. 1995, *AJ*, 109, 2757
- McWilliam, A. & Smecker-Hane, T. A. 2005, *ApJ*, 622, L29
- Milone, A. P., Piotto, G., Renzini, A., et al. 2017, *MNRAS*, 464, 3636
- Mishenina, T. V., Kovtyukh, V. V., Soubiran, C., Travaglio, C., & Busso, M. 2002, *A&A*, 396, 189
- Mishenina, T. V., Gorbaneva, T. I., Basak, N. Y., Soubiran, C., & Kovtyukh, V. V. 2011, *Astronomy Reports*, 55, 689
- Mucciarelli, A. & Bonifacio, P. 2020, *A&A*, 640, A87
- Myeong, G. C., Vasiliev, E., Iorio, G., Evans, N. W., & Belokurov, V. 2019, *MNRAS*, 1731
- Naidu, R. P., Conroy, C., Bonaca, A., et al. 2020, *ApJ*, 901, 48
- Norris, J., Cottrell, P. L., Freeman, K. C., & Da Costa, G. S. 1981, *ApJ*, 244, 205
- Norris, J. E. & Da Costa, G. S. 1995a, *ApJ*, 447, 680
- Norris, J. E. & Da Costa, G. S. 1995b, *ApJ*, 441, L81
- Odenkirchen, M., Grebel, E. K., Rockosi, C. M., et al. 2001, *ApJ*, 548, L165
- Pancino, E., Mucciarelli, A., Sbordone, L., et al. 2011, *A&A*, 527, A18
- Pilachowski, C. A., Sneden, C., & Kraft, R. P. 1996, *AJ*, 111, 1689
- Pillepich, A., Madau, P., & Mayer, L. 2015, *ApJ*, 799, 184
- Ramírez, I., Meléndez, J., & Chanamé, J. 2012, *ApJ*, 757, 164
- Reina-Campos, M., Hughes, M. E., Kruijssen, J. M. D., et al. 2020, *MNRAS*, 493, 3422
- Roederer, I. U. & Barklem, P. S. 2018, *ApJ*, 857, 2
- Roederer, I. U., Preston, G. W., Thompson, I. B., et al. 2014, *AJ*, 147, 136
- Romano, D., Matteucci, F., Tosi, M., et al. 2007, *MNRAS*, 376, 405
- Sarajedini, A. & Layden, A. C. 1995, *AJ*, 109, 1086
- Savino, A. & Posti, L. 2019, *A&A*, 624, L9
- Schlafly, E. F. & Finkbeiner, D. P. 2011, *ApJ*, 737, 103
- Searle, L. & Zinn, R. 1978, *ApJ*, 225, 357
- Shi, J. R., Yan, H. L., Zhou, Z. M., & Zhao, G. 2018, *ApJ*, 862, 71
- Simmerer, J., Sneden, C., Cowan, J. J., et al. 2004, *ApJ*, 617, 1091
- Simpson, J. D., Martell, S. L., Da Costa, G., et al. 2020, *MNRAS*, 491, 3374
- Sitnova, T. M., Mashonkina, L. I., & Ryabchikova, T. A. 2013, *Astronomy Letters*, 39, 126
- Smith, V. V., Cunha, K., & Lambert, D. L. 1995, *AJ*, 110, 2827
- Smith, V. V., Suntzeff, N. B., Cunha, K., et al. 2000, *AJ*, 119, 1239
- Sneden, C. A. 1973, PhD thesis, The University of Texas at Austin.
- Sneden, C., Lawler, J. E., Cowan, J. J., Ivans, I. I., & Den Hartog, E. A. 2009, *ApJS*, 182, 80
- Sobeck, J. S., Ivans, I. I., Simmerer, J. A., et al. 2006, *AJ*, 131, 2949
- Steinmetz, M., Zwitter, T., Siebert, A., et al. 2006, *AJ*, 132, 1645
- Suntzeff, N. B. & Kraft, R. P. 1996, *AJ*, 111, 1913
- Tang, B., Liu, C., Fernández-Trincado, J. G., et al. 2019, *ApJ*, 871, 58
- Valcarlos, A. A. R. & Catelan, M. 2011, *A&A*, 533, A120
- Villanova, S., Geisler, D., Gratton, R. G., & Cassisi, S. 2014, *ApJ*, 791, 107
- Zacharias, N., Finch, C. T., Girard, T. M., et al. 2013, *AJ*, 145, 44
- Zolotov, A., Willman, B., Brooks, A. M., et al. 2009, *ApJ*, 702, 1058